Monthly Notices
of the
ROYAL ASTRONOMICAL SOCIETY

MNRAS **462,** 421–428 (2016)
Advance Access publication 2016 July 5

doi:10.1093/mnras/stw1520

Early quenching of massive protocluster galaxies around $z = 2.2$ radio galaxies

K. Husband,[1] M. N. Bremer,[1⋆] J. P. Stott[2,3] and D. N. A. Murphy[4]

[1] *H.H. Wills Physics Laboratory, University of Bristol, Tyndall Avenue, Bristol BS8 1TL, UK*
[2] *Sub-department of Astrophysics, Department of Physics, University of Oxford, Denys Wilkinson Building, Keble Road Oxford OX1 3RH, UK*
[3] *Institute for Computational Cosmology, Durham University, South Road, Durham DH1 3LE, UK*
[4] *Instituto de Astrofísica, Pontificia Universidad Católica de Chile, Avenida Vicuña Mackenna 4860, Santiago, Chile*

Accepted 2016 June 21. Received 2016 June 21; in original form 2015 April 29

ABSTRACT

Radio galaxies are among the most massive galaxies in the high-redshift Universe and are known to often lie in protocluster environments. We have studied the fields of seven $z = 2.2$ radio galaxies with High Acuity Wide field K-band Imager (HAWK-I) narrow-band and broad-band imaging in order to map out their environment using Hα emitters (HAEs). The results are compared to the blank field HAE survey HiZELS. All of the radio galaxy fields are overdense in HAEs relative to a typical HiZELS field of the same area and four of the seven are richer than all except one of 65 essentially random HiZELS subfields of the same size. The star formation rates of the massive HAEs are lower than those necessary to have formed their stellar population in the preceding Gyr – indicating that these galaxies are likely to have formed the bulk of their stars at higher redshifts, and are starting to quench.

Key words: galaxies: clusters: general – galaxies: evolution – galaxies: high-redshift – galaxies: luminosity function, mass function.

1 INTRODUCTION

Overdensities of galaxies that are expected to be the progenitors of local massive galaxy clusters have been found around high-redshift radio galaxies (e.g. Venemans et al. 2004; Overzier et al. 2006; Hatch et al. 2011; Kuiper et al. 2011) and quasars (e.g. Venemans et al. 2007; Kim et al. 2009; Utsumi et al. 2010; Husband et al. 2013). These protoclusters are generally discovered via their star-forming population; in part because it is easier to get confirming spectroscopy of actively star-forming galaxies that contain emission lines, unlike passive galaxies, and in part because studies of low- and intermediate-redshift clusters indicate that the majority of stars in cluster galaxies formed at $z > 2$ (e.g. Ellis et al. 1997; Tran et al. 2007). This rapid growth in clusters at high redshift contrasts to that in low-redshift clusters where star formation is suppressed relative to the field. The redshift range over which their galaxy population becomes red and dead can be determined using a large sample of protoclusters selected through a range of techniques in order to minimize selection biases.

An efficient way of finding protoclusters at $z > 2$ appears to be through targeted searches around radio galaxies and quasars. The growth of galaxies is likely linked to the growth of their central black holes, and consequently AGN are expected to reside in protoclusters (Smail et al. 2003; Lehmer et al. 2009; Digby-North et al. 2010; Matsuda et al. 2011). This and the fact that powerful radio galaxies are generally among the most massive galaxies at any epoch (De Breuck et al. 2002; Seymour et al. 2007) make them ideal objects for targeted protocluster searches. There is already a significant body of work exploring radio galaxy environments through Hα emission such as that by Hatch et al. (2011) using High Acuity Wide field *K*-band Imager (HAWK-I) and ISAAC on the VLT and the Mahalo ('Mapping HAlpha and Lines of Oxygen with Subaru') project with Subaru (Kodama et al. 2013; Shimakawa et al. 2014) among others (e.g. Cooke et al. 2014). These Hα studies have often targeted known protoclusters discovered by other means (such as overdensities of red galaxies or BzKs) and may well be subject to publication bias where only the most overdense regions are followed up or published, giving little clue about the fraction of radio galaxies that reside in star-forming overdensities.

Powerful radio sources themselves significantly influence the evolution of galaxies within their host dark matter halo. Radio jets are known to stop gas cooling through the kinetic mode of feedback on galactic scales (McNamara & Nulsen 2007; Cattaneo et al. 2009) and powerful radio galaxies at high redshift, whose jets can extend over 100s of kpc, may also affect intra-group gas (Fabian 2012). Outflows from $z \sim 2$ radio galaxies may be observational evidence for radio jets interacting with the early intra-group or intra-cluster medium (Nesvadba et al. 2006, 2008). Such AGN feedback is essential in simulations to reproduce the observed anti-hierarchical

⋆ E-mail: m.bremer@bristol.ac.uk

Table 1. A summary of the HAWK-I imaging. The radio luminosities are from observations at 4.7 or 4.85 GHz. The NB filters used in this work were NB2090 ($\lambda_{mean} = 20954$ Å; covering Hα between $z = 2.178$ and 2.207), H2 ($\lambda_{mean} = 21248$ Å; covering Hα between $z = 2.215$ and 2.260) and Brγ ($\lambda_{mean} = 21643$ Å; covering Hα between $z = 2.275$ and 2.321). The *K* filter used was the *Ks* filter (central wavelength = 21 323 Å, FWHM = 3150 Å).

Field	RA	Dec.	Redshift	$L_{4.8GHz}$ (10^{26} W Hz^{-1})	NB filter	NB exposure [h (2σ AB)]	*K* exposure [h (2σ AB)]	NB seeing (arcsec)	K seeing (arcsec)
MRC 0200+015	02:02:42.9	+01:49:10	2.229	21.1	H2	3.33 (22.5)	0.66 (22.9)	0.59	0.68
NVSS J015640	01:56:40.4	−33:25:33	2.198	42.4	NB2090	3.33 (22.2)	0.66 (23.4)	0.60	0.64
PMN J0340−6507	03:40:44.9	−65:07:07	2.289	33.8	Brγ	4.70 (22.4)	0.66 (22.8)	0.70	0.74
NVSS J045226	04:52:26.6	−17:37:53	2.256	9.6	H2	4.00 (22.5)	0.66 (22.9)	0.55	0.72
NVSS J094748	09:47:48.4	−20:48:36	2.294	4.0	Brγ	3.33 (22.4)	0.66 (22.6)	0.54	0.77
NVSS J100253	10:02:53.1	+01:34:56	2.248	1.6	H2	3.33 (22.7)	0.66 (23.0)	0.58	0.59
MRC 1113−178	11:16:14.5	−18:06:22	2.239	30.0	H2	3.62 (22.2)	0.66 (23.3)	0.65	0.62

growth and local galaxy luminosity function (e.g. Bower et al. 2006). AGN feedback on extragalactic scales may increase the entropy and pressure of the gas in the local environment of massive galaxies cutting off the supply of cold gas, which would otherwise accrete on to the galaxies fuelling star formation, and resulting in relatively quiescent member galaxies relatively early on (Hatch et al. 2014).

In this work we have explored the ∼12 comoving Mpc scale environment of seven $z = 2.2$ radio galaxies with VLT/HAWK-I using Hα emitters (HAEs) selected through narrow-band (NB) imaging in order to study galaxy clustering around such objects. The seven radio galaxies were selected purely on their spectroscopic redshift (falling within the range of the HAWK-I NB filters) and availability from Chile on the dates of observations. They all have radio luminosities greater than 1×10^{26} W Hz^{-1} at 4.7–4.85 GHz observed. Selecting HAEs results in a relatively clean sample of galaxies within a narrow redshift range ($\Delta z = 0.05$) as Hα is less affected by dust extinction (or metallicity) compared to other strong lines (Koyama et al. 2013b). We use the same method as the HiZELS survey (Sobral et al. 2013) to select HAEs in order to have a field galaxy comparison sample.

A Λcold dark matter (ΛCDM) cosmology with $H_0 = 69.6$ km s^{-1} Mpc^{-1}, $\Omega_M = 0.286$ and $\Omega_\Lambda = 0.714$ (Bennett et al. 2014) is used throughout and all the magnitudes quoted are in the AB system (Oke & Gunn 1983).

2 DATA

2.1 Imaging and data reduction

The seven radio galaxy fields were imaged with HAWK-I on the VLT in 2012 Oct/Nov and 2013 Jan/Feb/Mar with the *J* filter, short *K* (*Ks*) filter and a NB filter centred on the wavelength of Hα from the radio galaxy (NB2090, H2 or Brγ). HAWK-I has a field of view of 7.5 by 7.5 arcmin^2 or 12.2 by 12.2 comoving Mpc^2 at these redshifts ($z = 2.23$). The average exposure time was 0.62, 0.71 and 3.7 h in *J*, *Ks* and the NB reaching 2σ depths of 22.9, 23.0 and 22.4 on average, respectively (see Table 1).

The radio galaxies were selected in an unbiased way from a narrow redshift range between $2.198 < z < 2.294$ to match the available NB filters. They lie over a range of RAs convenient for scheduling. Only the environment of MRC0200+015 has been studied before – it was found to be overdense in HAEs by van der Werf, Moorwood & Bremer (2000) and Matsuda et al. (2011) but our new observations are ∼1 mag deeper.

The data were reduced by first subtracting a dark frame from the images and then flat-fielding with an averaged, normalized twilight flat-field. The images were then normalized and median combined together without offsets to make another flat-field that was applied to all images to remove any remaining sky residuals. Finally, the images were combined with offsets, cosmic ray rejection (using sigma clipping) and a bad pixel mask in order to deal with the chip gaps. The images were calibrated using unsaturated and cleanly extracted 2MASS objects in the fields. The magnitudes of the objects were extracted in 2 arcsec diameter apertures using SExtractor (Bertin & Arnouts 1996).

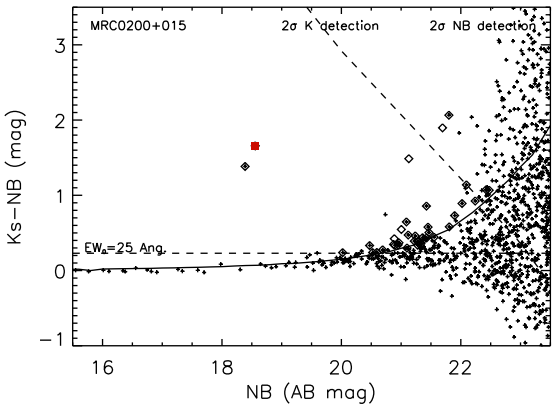

Figure 1. The *Ks*-NB versus NB colour–magnitude diagram for the MRC0200+015 radio galaxy field. The red square indicates the radio galaxy and the dashed lines show the 2σ limits on the imaging. Also shown are the EW limit and the line of three times the average observational error. The HAEs that were selected after visual inspection are highlighted by diamonds.

2.2 Hα emitter selection

We selected HAEs from a *Ks*-NB versus *Ks* colour–magnitude diagram (see e.g. the colour–magnitude diagram for MRC0200+015 in Fig. 1) in a similar manner to Sobral et al. (2013). Specifically, in this work HAEs are defined as galaxies with a *Ks*-NB colour greater than 3Σ (where Σ is the combined average error on the NB and *Ks*-band magnitudes at the NB magnitude), a NB magnitude brighter than the 2σ NB limiting magnitude, and a rest-frame NB equivalent width (EW) greater than 25 Å. All of the HAEs were individually checked to confirm that their sizes and morphologies were consistent with $z \sim 2$ galaxies rather than stars or artefacts. Fig. 2 shows some of the selected HAEs.

2.3 Hα star formation rates and equivalent widths

The star formation rates (SFRs) and EWs of the HAEs were calculated from the NB and *Ks* magnitudes, via the continuum flux

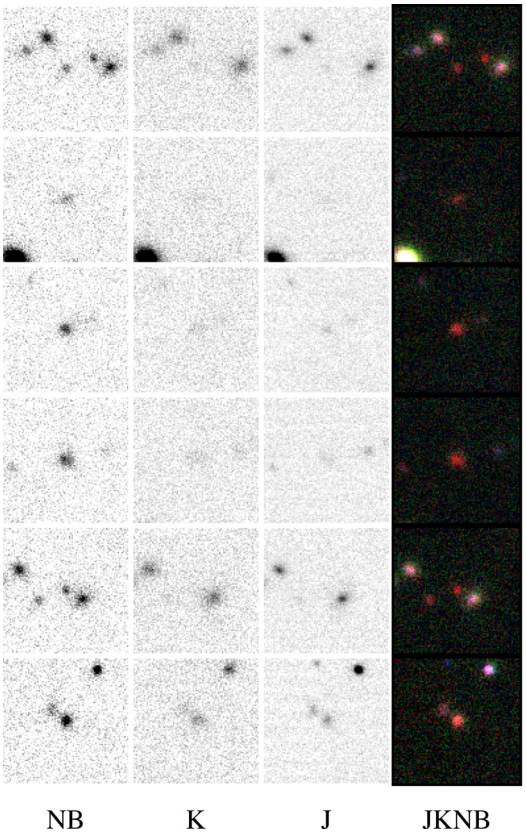

Figure 2. The NB, *Ks*, *J* and three colour-combined images of some of the HAEs selected (all taken from the NVSS J094748 radio galaxy field). The images are 10 by 10 arcsec across and the numbers on the right hand side are the NB AB magnitudes and the *Ks*-NB colours of the HAEs.

density per Angstrom, f_{Kc}, and Hα flux, $f_{\mathrm{H}\alpha}$, using the following equations (see e.g. Cooke et al. 2014):

$$f_{Kc} = \frac{w_K 10^{(-m_K-48.6)/2.5} - w_{\mathrm{NB}} 10^{(-m_{\mathrm{NB}}-48.6)/2.5}}{w_K - w_{\mathrm{NB}}} \quad (1)$$

$$f_{\mathrm{H}\alpha} = w_{\mathrm{NB}}(10^{(-m_{\mathrm{NB}}-48.6)/2.5} - f_{Kc}) \quad (2)$$

$$\mathrm{EW} = \frac{f_{\mathrm{H}\alpha}}{f_{Kc}(1+z)} \quad (3)$$

$$\mathrm{SFR} = 4\pi d^2 f_{\mathrm{H}\alpha} \times 4.39 \times 10^{-42}\ \mathrm{M}_\odot\ \mathrm{yr}^{-1} \quad (4)$$

where w_K and w_{NB} are the effective widths of the *Ks* and NB filters, m_K and m_{NB} are the *Ks* and NB AB magnitudes of the HAEs, $f_{\mathrm{H}\alpha}$ is the flux of Hα in erg s^{-1} cm^{-2}, d is the comoving radial distance in centimetres and z is the redshift of the HAEs, which is assumed to be the same as the radio galaxy. Equation (4) assumes that all of the photoionization is by young stars and not active galactic nuclei (AGN). If AGN are present then the estimates of SFR will be too high. However previous follow-up of HAEs with X-ray observations and rest-frame optical spectroscopy, in both clustered and non-clustered fields, indicates only a low (<10 per cent) fraction of HAEs contain AGN (see Hatch et al. 2011; Koyama et al. 2013b; Sobral et al. 2013; Stott et al. 2013). Hence, we do not expect this to significantly affect our results.

2.4 HAE masses

The masses of the HAEs were estimated from the observed *Ks*-band magnitudes, using a mass-to-light ratio with an additional $J - Ks$ colour term to take into account different star formation histories, following the method of Koyama et al. (2013b). Specifically:

$$\log(M_*/10^{11}\,\mathrm{M}_\odot) = -0.4(Ks - 22.24) + \Delta \log M \quad (5)$$

where

$$\Delta \log M = 0.14 - 0.9 \exp[-1.23(J - Ks)] \quad (6)$$

and M_* is the stellar mass, J and Ks are AB magnitudes, and assuming a Salpeter IMF. We then convert these to the equivalent Chabrier masses for consistency with equation (4). Koyama et al. (2013b) note that this 'one-colour method' agrees well with a full SED fitting method (with ∼0.3 dex scatter) over a wide range of luminosities (over nearly 3 mag).

Again if a HAE contains an optically bright AGN then the estimate of its mass will be too high, but we do not expect a large AGN fraction (see the previous and next section) and so this should not significantly affect our results.

2.5 Contamination

The final sample of HAEs could be contaminated by emission line galaxies such as [OIII] emitters at $z \sim 3$ or Pa series emitters at lower redshifts. The higher redshift interlopers are likely very rare (for example only 1 of 55 HAEs satisfied a $z \sim 3$ LBG selection in Geach et al. 2008) and broad-band selections such as the BzK selection (Daddi et al. 2004) can remove the lower redshift interlopers. In previous studies the majority (>90 per cent) of HAEs were found to lie within the BzK selection (Koyama et al. 2013b; Sobral et al. 2013). Due to this and the paucity of deep ancillary multi-wavelength data in these fields we do not apply additional broad-band selections (such as BzK) here as Sobral et al. (2013) have shown it to be unnecessary. As the probability for any one HAE detection to be a contaminant is small ($\lesssim$10 per cent), the probability for a group of contaminant galaxies to align with the radio galaxy is very small, and hence we believe contaminants do not significantly affect this work.

3 RESULTS AND DISCUSSION

3.1 Radio galaxy environments

The positions of the HAEs in the two richest and the poorest radio galaxy fields are shown in Fig. 3. The number of HAEs found in each field is detailed in Table 2. As the image depth varies between fields, the number of HAEs in each field using an identical selection is also shown in the table having applied the selection function of the shallowest field, NVSS J094748, and corrected the NB magnitudes to those expected if the same NB filter was used as the NVSS J094748 field.

In order to understand the significance of any clustering in the radio galaxy fields, we can compare the number of HAEs in each field to those derived from the much larger area HiZELS observations carried out with UKIRT (Sobral et al. 2013). HiZELS imaged 2.3 deg^2 of COSMOS and UDS to a similar depth as the radio galaxy fields and selected HAEs at the same redshift with similar criteria and the same EW limit as this work. However, HiZELS uses a smaller width NB filter and hence probes only ∼0.7 times the volume per unit area in comparison to the observations of

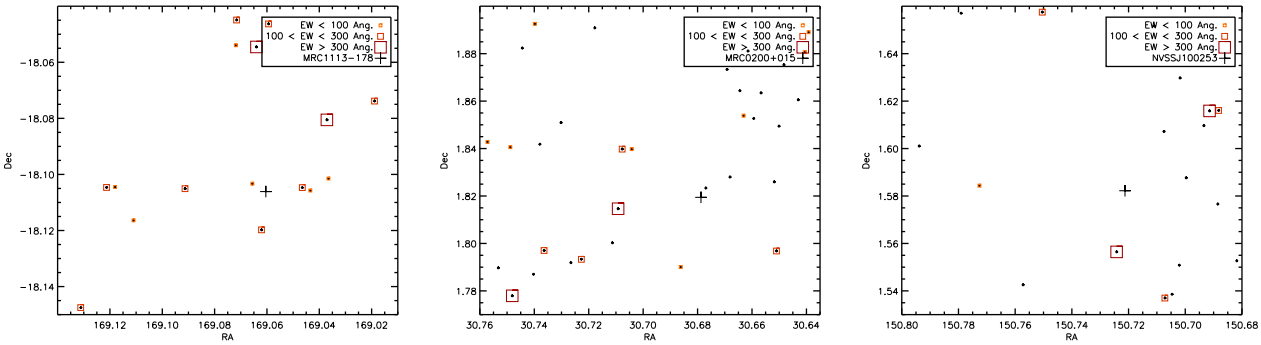

Figure 3. The distribution of HAEs that meet the NVSS J094748 selection criteria in the two richest (left and middle) and the poorest (right) of the radio galaxy fields. The size and colour of the point indicate the EW of the HAE. The small crosses indicate HAEs that do not meet the NVSS J094748 selection criteria. At this redshift 0.″01 corresponds to 0.97 comoving Mpc.

Table 2. A summary of the number of galaxies and relative overdensity detected in each field. Brackets denote the raw number of galaxies measured in the fields, NVSS J015640 and HiZELS, that have been corrected for the narrower filter widths. [1]The selection of the shallowest field, NVSS J094748, is applied to all fields so a direct comparison can be made. [2]Note that the overdensity is calculated to be the number of galaxies in excess of the background, i.e. $\rho_g = (\rho_{rg} - \rho_{bkg})/\rho_{bkg}$ where ρ_{rg} is the surface density of galaxies in the protocluster fields and ρ_{bkg} is the surface density of background galaxies calculated from the HiZELS survey using the same HAE selection as the NVSS J094748 field (Rigby et al. 2014). The upper limit to the expected eventual mass of a system at $z = 0$ is calculated using the matter overdensity method discussed in the text The errors on these masses are calculated taking account of the statistical uncertainty on the number of excess HAEs measured in each field.

Field	No. of HAEs	No. of HAEs to same limit[1]	No. of bright HAEs ($L_{H\alpha} > 10^{43}$ erg s^{-1})	Overdensity[2], ρ_g (excess)	Mass at $z = 0$ (10^{14} M$_\odot$)
MRC 0200+015	39	14	5	3.2 ± 1.1	12 ± 4.3
NVSS J015640	10	7.8 (5)	3 (2)	1.4 ± 0.9	3.2 ± 2.0
PMN J0340−6507	24	8	5	1.4 ± 0.9	5.4 ± 3.2
NVSS J045226	32	12	5	2.6 ± 1.1	8.4 ± 3.4
NVSS J094748	13	13	4	2.9 ± 1.1	6.3 ± 2.4
NVSS J100253	18	5	1	0.8 ± 0.7	2.7 ± 2.5
MRC 1113−178	16	16	10	3.9 ± 1.2	12 ± 3.9
Radio galaxy mean	23.4	11.0	4.6	2.3	7.2
HiZELS	na	3.3 (2.4)	0.6 (0.4)	na	na

all radio galaxy fields except that of NVSS J015640. The difference in filter widths also results in a different relationship between $K_s - NB$ colour and line EW. In all of the following we scale the HiZELS-derived numbers to the volume and EW sensitivity of our data.

We explore the strength of clustering by a simple counts in cells analysis, each cell being the size of a HAWK-I field. We determine the number of line emitters that would meet our NVSS J094748 selection criteria having taken into account the different width NB filters used in the two sets of observations. We place the cells on to the HiZELS data in two ways. First, we simply divide the HiZELS surveys into 88 equal-area, non-overlapping squares or cells. As this does not take into account any intrinsic clustering in the $z = 2.2$ galaxy distribution, we secondly amend the positioning of each cell so that it is centred on a HAE (to mimic the effect of the HAWK-I fields being centred on known $z = 2.2$ galaxies) while ensuring the cells still do not overlap. This necessarily reduces the number of cells to 65 as the spatial distribution of HAEs does not allow for as efficient abutting of cells as simply splitting the entire survey area uniformly. In reality, the difference in the statistics derived from the two approaches is very similar with the mean number of sources per cell meeting our selection criteria increased by only ∼30 per cent when they are centred on HAEs. We use the statistics derived from the second approach in the following analysis.

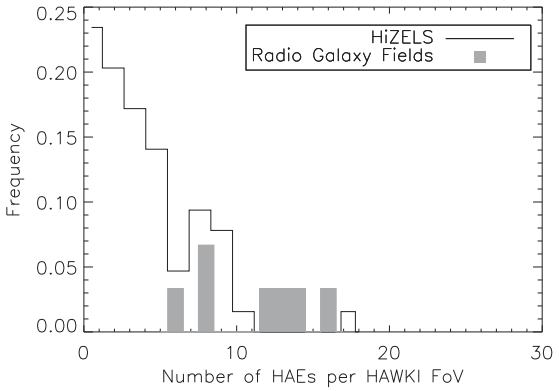

Figure 4. The number of HAEs meeting our selection criteria around non-overlapping HAWK-I sized pointings centred on HAEs in the HiZELS fields (COSMOS+UDS). The number of HAEs around the radio galaxies is shown by grey-filled bins whose frequency is set to an arbitrary level.

The distribution of the number of HAEs per HAWK-I field derived from HiZELS is shown in Fig. 4. The volume density of HAEs derived from the HiZELS data translates to a mean surface density of 3.3 per HAWK-I survey field. As summarized in Table 2 the radio galaxy fields are on average three times denser than the HiZELS

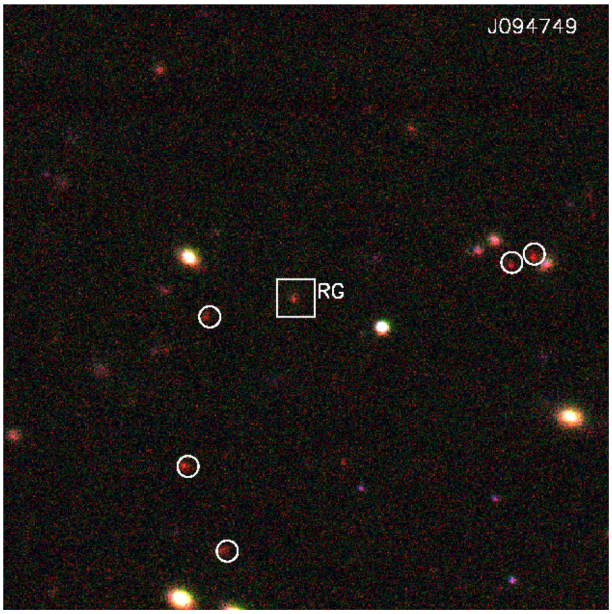

Figure 5. The 1 by 1 arcmin^2 NB image of the centre of the NVSS J094748 field (the online journal shows the three-colour, *JKsNB*, image). The radio galaxy is marked by a square and the redder HAEs that meet our selection criteria are circled.

survey fields and one field (MRC1113-178) in particular contains nearly five times the number of HAEs than the mean HiZELS value. The highest density field out of the 65 in the HiZELS distribution (the cell with 17 HAEs) is contributed by a single structure in one of the two HiZELS fields. This structure has been discussed by Geach et al. (2012) and is likely to turn into a significant cluster at $z = 0$. While it does not contain any radio source of comparable luminosity to those studied here, it does contain a quasar at the same redshift.

Although the HAWK-I field of view is well-matched to the predicted effective radius of protoclusters from the Millennium Simulation (∼6 comoving Mpc; Chiang, Overzier & Gebhardt 2013), some sub-clustering is expected particularly near the central massive object. Indeed, in some fields the overdensity is much larger if we consider a smaller scale. In particular, in the NVSS J094748 field the HAEs appear to cluster around the radio galaxy (see Fig. 5). In a 1 arcmin^2 area there are five HAEs plus the radio galaxy compared to an expectation of ∼0.2 HAEs per arcmin^{-2} from the HiZELS survey – only one of the HAEs in HiZELS has more HAEs within a 1 by 1 arcmin^2 box centred on them when scaled to the same volume, indicating that the radio galaxy is at the centre of a dense structure that perhaps evolves into a massive galaxy by the present day.

Given these results, the typical radio galaxy field contains a clear excess of star-forming galaxies relative to the survey fields in line with the literature (e.g. Hatch et al. 2011; Kuiper et al. 2011), but with significant variations from field to field. We find four out of seven (around 60 per cent) of the radio galaxy fields to be denser than 98 per cent (and all of the radio galaxy fields to be denser than 80 per cent) of similar-sized regions in HiZELS at $z = 2.23$ when scaled to the same volume per unit area. This is a similar result to Venemans et al. (2007) who found that six out of eight of the $z > 2$ radio galaxies in their sample were surrounded by an overdensity of Lyα emitters. However, from Fig. 4 it is clear that, on average, radio galaxies at $z = 2$ do not lie in the most extreme ($>5\sigma$) overdensities – the existence of the Geach et al. (2012) system within the HiZELS fields demonstrates this.

Assuming that these overdensities could develop into current-day group and clusters, it is instructive to estimate the likely eventual masses of these systems. This can be done by estimating the matter overdensity they represent, which in turn is related to the galaxy overdensity measured through the galaxy bias, b (following e.g. Venemans et al. 2007). For HAEs at this redshift, selected in a similar manner to ours down to a SFR limit of 20 M$_\odot$ yr^{-1}, the bias is measured to be around 2.4 (Geach et al. 2012). If we assume that all the matter within the volume will collapse into a cluster by the present day, then the final mass of the system is just the volume (∼5000 comoving Mpc^3) times the matter overdensity times the critical density of the universe. This gives $z = 0$ masses of at most several times 10^{14} M$_\odot$ (see Table 2). However, these values must be taken as upper limits as it is improbable that everything within the volume probed will collapse into the eventual structure. The mass of these systems can also be estimated independently by mapping their apparent number density on to the current-day cluster mass function. As there is at most one system of similar or greater density to the most clustered radio galaxy field in the 2.34 deg^2 of HiZELS, the number density of such systems must be around or less than 1×10^{-6} Mpc^{-3}, implying the eventual mass of the richest of the systems studied here would be $\sim 5 \times 10^{14}$ M$_\odot$ using the Tinker et al. (2008) $z = 0$ halo mass function of clusters. Given the inevitable scatter in the mass growth of individual structures between $z \sim 2$ and today, both mass estimates are consistent and imply the systems have the potential to become systems characterized as rich groups or moderate-mass clusters today.

There have been numerous previous studies of radio galaxy environments at $z \sim 2$ using HAEs to map out the local galaxy densities (e.g. Kurk et al. 2004; Hatch et al. 2011; Hayashi et al. 2012; Koyama et al. 2013a; Cooke et al. 2014). The estimated final masses of these systems are again generally around a few times 10^{14} M$_\odot$ using the galaxy bias prescription, with the exception of the protocluster around the Spiderweb galaxy whose eventual mass is estimated to be nearly 10^{15} M$_\odot$ (both using this method and other methods based on additional data such as spectroscopic velocities and X-ray observations detailed in Shimakawa et al. 2014).

3.2 Luminosity and mass functions

The Hα luminosity function is shown in Fig. 6 along with the luminosity function of field galaxies from Sobral et al. (2012). The Hα fluxes have been corrected for [N II] emission that is likely to fall into the NB filter. This was carried out using an empirically derived relation between the ratio of [N II] to Hα and the sum of their EWs taken from Sobral et al. (2012). The median value of the [N II]/(Hα+[N II]) ratio is 0.16. In addition, Sobral et al. (2009) have demonstrated that the wavelength response of similar filters is sufficiently close to a 'top-hat' profile that any difference has a minimal effect on the calculated luminosity function. Hence, we do not correct for the filter profile.

Numerous studies have indicated that HAEs are dust extincted by around $A_{\rm H\alpha} = 1.0$ mag and that the amount of dust extinction does not significantly change with luminosity (e.g. Garn et al. 2010; Sobral et al. 2012), although there is some evidence that the amount of dust correction may slightly depend on mass (e.g. Shimakawa et al. 2015, see below). We follow Sobral et al. (2013) and apply one magnitude of dust extinction to all of our HAEs. This will increase the SFRs inferred for the objects using the relation given in

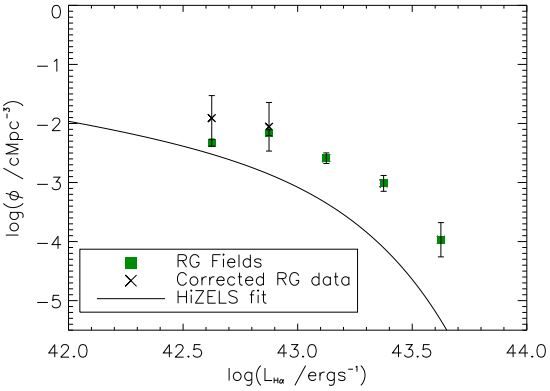

Figure 6. Hα luminosity function for the radio galaxy fields with the $z = 2.23$ fit from the HiZELS survey work (Sobral et al. 2013) shown as a black line. The green filled squares are the observed luminosity densities and crosses are the values corrected for incompleteness following the prescription of Sobral et al. (2013) which appreciably affects only the two lowest luminosity bins. The error bars are generated as described in the text.

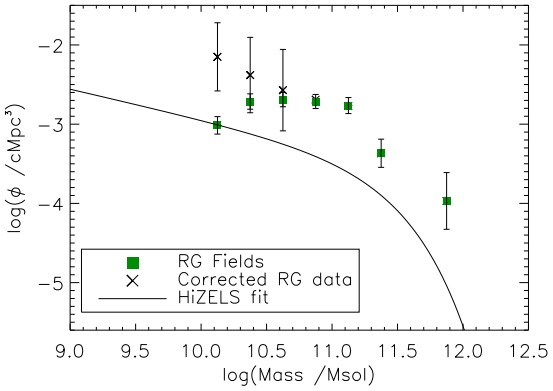

Figure 7. Mass function of the HAEs in the radio galaxy fields with the field line from the HiZELS survey (Sobral et al. 2013) at $z = 2.23$. The raw values are shown as green boxes and the completeness-corrected values are shown as crosses. There is a clear excess of galaxies in the radio galaxy fields, which, once completeness is corrected for, is consistent in shape with that of the HiZELS mass function, albeit offset by a factor of ∼3–5 (see Table 2).

Section 2.4 but will not affect the masses as this relation is based on the observed *Ks* magnitude.

In order to calculate the errors on the luminosity function, we performed a Monte Carlo simulation whereby each HAE candidate was simulated a thousand times with the *Ks* band and *NB* magnitudes taken from a Gaussian distribution centred on the observed magnitudes with a width equal to the error on the photometry. Assuming Poisson statistics, the error on a particular luminosity bin is the square root of the mean number of simulated HAEs falling within that bin (see below; this follows the method of Sobral et al. 2012). The lowest luminosity bins are affected by incompleteness and we correct for this using the prescription of Sobral et al. (2013).

The Hα luminosity function shows an excess of HAEs in the radio galaxy fields compared to HiZELS. This is not due to the radio galaxies themselves, which are excluded from the luminosity function to avoid biasing the results as the rarity of radio galaxies means they are not likely to contribute significantly to the HiZELS results.

The dust correction used may subtly change the shape of the luminosity function. Consequently, if a mass-dependent dust correction (as suggested in Shimakawa et al. 2015) is applied to the data instead of a uniform dust correction for all objects the luminosity function will flatten, increasing the number of HAEs with high Hα luminosities. However, this will not affect the *excess* of bright objects seen around radio galaxies compared to the field, unless there is a different dust–stellar mass relation in these dense regions compared to the field.

The HAE mass function is shown in Fig. 7. This is again compared to the field as determined from HiZELS (smooth black line; Sobral et al. 2013), which uses SED fitting to determine the mass of the HAEs. We see an excess of galaxies compared to HiZELS, as expected, that follows a similar shape to the HiZELS mass function at high mass but again, the lowest mass bins are affected by incompleteness. In order to correct the mass function without assuming the distribution of HAEs in mass or luminosity-EW space from HiZELS, we use equation (5) to estimate the mass of the HAEs as a function of *Ks*-band magnitude assuming a constant correction factor (equation 6) of −0.123 (i.e. assuming $J - K = 1$ – approximately the average colour of the HAEs). The fraction of sources recovered from the reduced *Ks* images at each magnitude was estimated by injecting circular, Gaussian-profiled sources into the images, running SExtractor and measuring the number recovered. From this the fraction of HAEs likely to have been missed per mass-bin was estimated and the measured number density increased by the inverse of this fraction. These corrections were significant for the three lowest mass bins, ranging from 0.15 dex for the third lowest to 0.9 dex for the lowest. Having applied this correction, the *shape* of the mass function in the radio galaxy is consistent within the uncertainties with that of HAEs in the general field. We note that previously Koyama et al. (2013a) and Cooke et al. (2014) found excesses of line emitters in two radio galaxy fields appeared to be confined to the most massive galaxies.

Thus, this work along with other studies with similar findings (Steidel et al. 2005; Hatch et al. 2011; Koyama et al. 2013b; Cooke et al. 2014) demonstrates that protocluster fields, such as those around radio galaxies, contain an excess of massive star-forming galaxies with comparatively high SFRs over those selected in the same manner from the same volume (at the same redshift) in the field.

3.3 HAE properties

The previous two sections have shown that the volume density of star-forming galaxies is higher in the immediate environment of radio galaxies than in the field. Once completeness corrections have been applied, the shape of both the Hα luminosity and stellar mass functions for the line emitters derived in this work is consistent with those of the field.

Fig. 8 shows the distribution of observed SFRs derived from Hα for the radio galaxy fields and for the HiZELS survey field when the same NVSS J094748 selection is applied to both fields and the HiZELS values degraded to the same uncertainties for a given flux/SFR as that of the radio galaxy field data. The mean SFR is higher in the radio galaxy fields (68 ± 15 versus 42 ± 3 $M_{\odot}yr^{-1}$ for HiZELS). A KS test on the two SFR distributions cannot reject at any level of significance that they are drawn from the same population, unsurprising given the similarity in shape of the two Hα luminosity functions once incompleteness has been corrected for.

Despite the similarities in the shapes of the HAE line luminosity and stellar mass functions for the radio galaxy fields and HiZELS once corrected for incompleteness, we find more low EW HAEs in the radio galaxy fields than in HiZELS (see Fig. 9) (the median EW

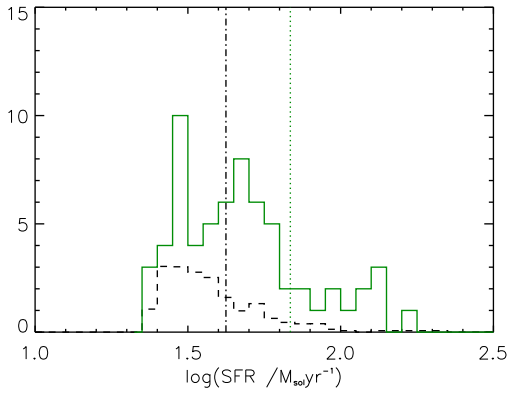

Figure 8. Histogram of the Hα SFRs of HAEs in the radio galaxy fields and the HiZELS field (scaled to the same volume as the sum of the radio galaxy fields) with the mean of each distribution overplotted. Both samples have had the same HAE selection (from the NVSS J094748 field) applied. The mean SFR is higher in the radio galaxy fields, but a KS test cannot distinguish between the distributions at any significant level.

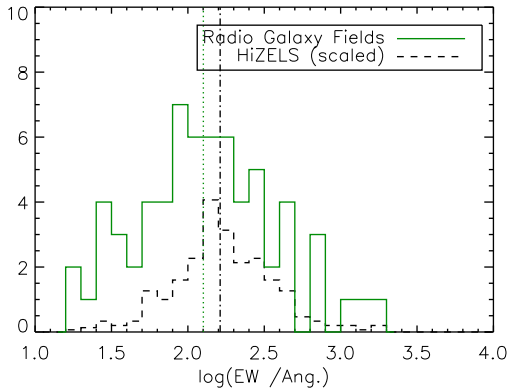

Figure 9. Histogram of the Hα EW of HAEs in the radio galaxy fields and the HiZELS field (scaled to the same volume as the sum of the radio galaxy fields) with the median of each distribution overplotted. Again, both samples have had the same HAE selection (from the NVSS J094748 field) applied. We find more low EW HAEs in the radio galaxy fields compared to the HiZELS survey fields, largely due to the excess of high-mass (and luminosity) HAEs in these fields.

for the radio galaxy and survey fields when an identical selection is applied is 163 ± 13 Å and 120 ± 40 Å, respectively.). The differences can in part be explained by the effect of incompleteness on the lower mass HAEs – low mass, low EW HAEs are not detected and/or selected in both our observations, and to a lesser extent in HiZELS, as they lie below the curved selection line in colour–magnitude space (see Fig. 1). However, the lack of high-mass *and* high EW HAEs in the radio galaxy fields and illustrated in the same figure is real – we see only one HAE with an NB magnitude brighter than 20 and $K - NB > 1$ excluding the radio galaxies. If the high-mass objects had the same range of EW as for the lower mass objects, they would have been selected.

The rest-frame EW measures the specific star formation rate (sSFR; the SFR per unit stellar mass) of the galaxies. For the objects meeting our selection, the mean sSFR for the massive ($M > 10^{10}$ M$_\odot$) HAEs is $\sim 1 \times 10^{-9}$ yr^{-1}, around the lower edge of the so-called main sequence of star formation at this redshift (Elbaz et al. 2011; Karim et al. 2011; Rodighiero et al. 2014) and less at higher mass ($\sim 7 \times 10^{-10}$ yr^{-1} at $M > 10^{10.5}$ M$_\odot$ and $\sim 4 \times 10^{-10}$ yr^{-1} at $M > 10^{11}$ M$_\odot$). Elbaz et al. (2011) derive a mean sSFR of $\sim 2.5 \times 10^{-9}$ for the main sequence of star-forming galaxies at $z = 2.25$. In other words, the sSFR in these relatively strongly star-forming galaxies appears somewhat suppressed (by around 0.3–0.8 dex) relative to the main sequence of star formation at this redshift. A similar result was found in Hatch et al. (2011) in two $z \sim 2$ radio galaxy fields and in Cooke et al. (2014) in a $z = 2.5$ radio galaxy field, although Cooke et al. (2014) note that this difference goes away when both samples are cut to stellar masses greater than 10^{10} M$_\odot$. If so, the relatively low sSFR seen in these massive galaxies could simply be related to mass (through downsizing where more massive galaxies tend to form their stars earlier and quicker than less massive galaxies) and not dependent on environment.

Given the evidence for completed red sequences in clusters at $z \sim 1.5$ (see e.g. De Propris, Bremer & Phillipps 2015) and for very early completion of star formation in the most massive cluster galaxies (e.g. Blakeslee et al. 2003; Mei et al. 2006) present-day galaxies with stellar masses comparable to those found in these overdensities appear to form their stellar populations early ($z \gtrsim 2.5$; consistent with stars in the most massive galaxies forming earlier than those in the bulk of other galaxies) and over a short period of time, typically less than 10^9 years (Thomas et al. 2010), or a sSFR of >1 Gyr^{-1}. Assuming the same time-scale for the most massive HAEs studied here, a minimum *average* SFR to build 10^{11} M$_\odot$ over this time would be at least 100 M$_\odot$ yr^{-1}, similar to or larger than the measured sSFR of the HAEs in the radio galaxy fields. If, as is likely, star formation varied stochastically during formation, the bulk of the stellar population will have formed during periods with significantly higher sSFRs than the values observed here. Consequently, even though these overdensities of HAEs are identified through ongoing significant star formation, many of the galaxies with masses $>10^{10}$ M$_\odot$ are likely to be past their peak in star formation (the HAEs are observed to lie below the main sequence at this redshift), and therefore likely to be in the process of quenching on their way to becoming the passively evolving systems observed in the cores of groups and clusters at lower redshifts.

While this reduced star formation at this epoch may be a feature of the evolution of massive galaxies in general it is worth exploring whether, in the case of the galaxies in these fields, the presence of a powerful radio galaxy in their immediate environment may be affecting their ongoing star formation. If the radio galaxy is affecting its local environment through heating of surrounding gas or through direct ionization from the AGN we may expect that the properties of the surrounding HAEs to change with distance from the central radio galaxy. However, we find no trend of *Ks* magnitude, *Ks*-NB colour, EW or SFR with projected distance from the central radio galaxy. We also find no trend of *Ks* magnitude, *Ks*-NB magnitude, EW or SFR with environmental density (calculated as the number of HAEs within a 30 arcsec radius). Thus, there is no evidence in this data of the radio galaxy affecting star formation in neighbouring galaxies through proximity to that galaxy. This is unsurprising as the observed fields (and therefore the scale length of the overdensities) are much larger than the extent of the radio emission from the radio galaxies.

4 CONCLUSIONS

We have studied the environment of seven $z = 2.2$ radio galaxies with broad and NB imaging from VLT/HAWK-I designed to select Hα emitting galaxies (HAEs) at the radio galaxy redshifts. We find the following.

(i) All seven fields show a clear excess of HAEs relative to the expected surface density derived from field surveys. In particular, four of the seven fields are denser than 98 per cent of similar-sized regions in the HiZELS survey. One field in particular is very

tightly clustered; the 1 arcmin^2 centred on the radio galaxy NVSS J094748 contains a density of HAEs so high that it is found only once over the same scale in the entire HiZELS survey. The fields of the other radio galaxies are overdense in HAEs spread across the wider HAWK-I field. The environments of the radio galaxies have properties consistent with those expected of the progenitors of rich groups and moderate-mass clusters in the current-day universe. Nevertheless, more richly clustered systems can be found in the $z \sim 2$ field (e.g. Geach et al. 2012). The *shapes* of the Hα luminosity and HAE mass functions are indistinguishable from those of the field; the difference appears to be in their normalization.

(ii) The excess of HAEs in the radio galaxy fields is evident across the range of the HAE mass function probed here, including high-mass galaxies – indicative of significant prior growth of these systems. The median sSFR for these massive ($M > 10^{10}$ M$_\odot$) HAEs is $\sim 10^{-9}$ yr^{-1} (around the lower edge of the main sequence of star formation at this redshift) and decreases with increasing mass. Given the time-scale over which these galaxies form their stellar populations is expected to be less than a Gyr, these sources or their progenitors are likely to have previously been forming stars at higher rates than those observed. Hence, these are massive galaxies undergoing (for them) moderate star formation at the observed epoch.

(iii) There is no evidence of the star formation in individual galaxies being affected by proximity to a radio galaxy based on a study of the star-forming parameters as a function of projected distance from the radio galaxy.

ACKNOWLEDGEMENTS

We would like to thank the anonymous referee for their extremely helpful comments that significantly improved this paper. We would also like to thank Nina Hatch for helpful discussions about this work. KH acknowledges funding from STFC. JPS acknowledges support from STFC (ST/I001573/1) and a Hintze Fellowship. DNAM acknowledges support through FONDECYT grant 3120214. This work is based on observations made with ESO Telescopes at the La Silla and Paranal Observatory under programme IDs 090.A-0387(ABC), 081.A-0932(A) and 083.A-0826(A). The astronomical table manipulation and plotting software TOPCAT (Taylor 2005) was used in the analysis of these data. We use the publicly available HiZELS catalogues from Sobral et al. (2013).

REFERENCES

Bennett C. L., Larson D., Weiland J. L., Hinshaw G., 2014, ApJ, 794, 135
Bertin E., Arnouts S., 1996, A&AS, 117, 393
Blakeslee J. P. et al., 2003, ApJ, 596, L143
Bower R. G., Benson A. J., Malbon R., Helly J. C., Frenk C. S., Baugh C. M., Cole S., Lacey C. G., 2006, MNRAS, 370, 645
Cattaneo A. et al., 2009, Nature, 460, 213
Chiang Y.-K., Overzier R., Gebhardt K., 2013, ApJ, 779, 127
Cooke E. A., Hatch N. A., Muldrew S. I., Rigby E. E., Kurk J. D., 2014, MNRAS, 440, 3262
Daddi E., Cimatti A., Renzini A., Fontana A., Mignoli M., Pozzetti L., Tozzi P., Zamorani G., 2004, ApJ, 617, 746
De Breuck C., van Breugel W., Stanford S. A., Röttgering H., Miley G., Stern D., 2002, AJ, 123, 637
De Propris R., Bremer M. N., Phillipps S., 2015, MNRAS, 450, 1268
Digby-North J. A. et al., 2010, MNRAS, 407, 846
Elbaz D. et al., 2011, A&A, 533, A119
Ellis R. S., Smail I., Dressler A., Couch W. J., Oemler A., Jr, Butcher H., Sharples R. M., 1997, ApJ, 483, 582
Fabian A. C., 2012, ARA&A, 50, 455
Garn T. et al., 2010, MNRAS, 402, 2017
Geach J. E., Smail I., Best P. N., Kurk J., Casali M., Ivison R. J., Coppin K., 2008, MNRAS, 388, 1473
Geach J. E., Sobral D., Hickox R. C., Wake D. A., Smail I., Best P. N., Baugh C. M., Stott J. P., 2012, MNRAS, 426, 679
Hatch N. A. et al., 2011, MNRAS, 410, 1537
Hatch N. A. et al., 2014, MNRAS, 445, 280
Hayashi M., Kodama T., Tadaki K.-i., Koyama Y., Tanaka I., 2012, ApJ, 757, 15
Husband K., Bremer M. N., Stanway E. R., Davies L. J. M., Lehnert M. D., Douglas L. S., 2013, MNRAS, 432, 2869
Karim A. et al., 2011, ApJ, 730, 61
Kim S. et al., 2009, ApJ, 695, 809
Kodama T., Hayashi M., Koyama Y., Tadaki K.-i., Tanaka I., Shimakawa R., 2013, in Thomas D., Pasquali A., Ferreras I., eds, IAU Symp. Vol. 295. IAU Symposium, p. 74
Koyama Y., Kodama T., Tadaki K.-i., Hayashi M., Tanaka M., Smail I., Tanaka I., Kurk J., 2013a, MNRAS, 428, 1551
Koyama Y. et al., 2013b, MNRAS, 434, 423
Kuiper E. et al., 2011, MNRAS, 415, 2245
Kurk J. D., Pentericci L., Overzier R. A., Röttgering H. J. A., Miley G. K., 2004, A&A, 428, 817
Lehmer B. D. et al., 2009, ApJ, 691, 687
McNamara B. R., Nulsen P. E. J., 2007, ARA&A, 45, 117
Matsuda Y. et al., 2011, MNRAS, 416, 2041
Mei S. et al., 2006, ApJ, 644, 759
Nesvadba N. P. H., Lehnert M. D., Eisenhauer F., Gilbert A., Tecza M., Abuter R., 2006, ApJ, 650, 693
Nesvadba N. P. H., Lehnert M. D., De Breuck C., Gilbert A. M., van Breugel W., 2008, A&A, 491, 407
Oke J. B., Gunn J. E., 1983, ApJ, 266, 713
Overzier R. A. et al., 2006, ApJ, 637, 58
Rigby E. E. et al., 2014, MNRAS, 437, 1882
Rodighiero G. et al., 2014, MNRAS, 443, 19
Seymour N. et al., 2007, ApJS, 171, 353
Shimakawa R., Kodama T., Tadaki K.-i., Tanaka I., Hayashi M., Koyama Y., 2014, MNRAS, 441, L1
Shimakawa R., Kodama T., Tadaki K.-i., Hayashi M., Koyama Y., Tanaka I., 2015, MNRAS, 448, 666
Smail I., Scharf C. A., Ivison R. J., Stevens J. A., Bower R. G., Dunlop J. S., 2003, ApJ, 599, 86
Sobral D. et al., 2009, MNRAS, 398, 75
Sobral D., Best P. N., Matsuda Y., Smail I., Geach J. E., Cirasuolo M., 2012, MNRAS, 420, 1926
Sobral D., Smail I., Best P. N., Geach J. E., Matsuda Y., Stott J. P., Cirasuolo M., Kurk J., 2013, MNRAS, 428, 1128
Steidel C. C., Adelberger K. L., Shapley A. E., Erb D. K., Reddy N. A., Pettini M., 2005, ApJ, 626, 44
Stott J. P. et al., 2013, MNRAS, 436, 1130
Taylor M. B., 2005, in Shopbell P., Britton M., Ebert R., eds, Astronomical Society of the Pacific Conference Series Vol. 347. ADASS XIV. Astron. Soc. Pac., San Francisco, p. 29
Thomas D., Maraston C., Schawinski K., Sarzi M., Silk J., 2010, MNRAS, 404, 1775
Tinker J., Kravtsov A. V., Klypin A., Abazajian K., Warren M., Yepes G., Gottlöber S., Holz D. E., 2008, ApJ, 688, 709
Tran K.-V. H., Franx M., Illingworth G. D., van Dokkum P., Kelson D. D., Blakeslee J. P., Postman M., 2007, ApJ, 661, 750
Utsumi Y., Goto T., Kashikawa N., Miyazaki S., Komiyama Y., Furusawa H., Overzier R., 2010, ApJ, 721, 1680
van der Werf P. P., Moorwood A. F. M., Bremer M. N., 2000, A&A, 362, 509
Venemans B. P. et al., 2004, A&A, 424, L17
Venemans B. P. et al., 2007, A&A, 461, 823

This paper has been typeset from a TEX/LATEX file prepared by the author.